

## Article

# Distribution and Genesis of Potassium-Bearing Minerals in Lop Nor Playa, Xinjiang, China

Kai Wang<sup>1,2</sup>, Yu Zhang<sup>3</sup>, Jiahuan Han<sup>4</sup>, Lichun Ma<sup>2,\*</sup>, Mianping Zheng<sup>2,\*</sup>, Yue Wu<sup>1</sup> and Banwang Yang<sup>5</sup><sup>1</sup> School of Earth Sciences and Resources, China University of Geosciences, Beijing 100083, China<sup>2</sup> MNR Key Laboratory of Saline Lake Resources and Environment, Institute of Mineral Resources, CAGS, Beijing 100037, China<sup>3</sup> Department of Earth Sciences, University College London, Gower Street, London WC1E 6BT, UK<sup>4</sup> College of Geosciences and Surveying Engineering, China University of Mining and Technology, Beijing 100083, China<sup>5</sup> Qinghai Forth Geological Exploration Institute, Xining 810000, China

\* Correspondence: mlchun@cags.ac.cn (L.M.); zhengmp2010@126.com (M.Z.)

**Abstract:** Lop Nor Playa is the main salt-forming area in the Tarim Basin, which is rich in brine resources. There is a large amount of potassium fertilizer produced from potassium-rich brine in Lop Nor annually, which meets about half of the demands of China's agricultural potash, along with that produced in the Qaidam Basin. In order to investigate the distribution characteristics of potassium-bearing minerals and the origin of potassium-bearing salts in Lop Nor Playa, mineralogy and hydrogeochemistry studies were carried out. The results showed that there are a large number of polyhalite layers distributed in the Luobei Depression and Xinqing Platform. Brines with high content of K<sup>+</sup> and Mg<sup>2+</sup> have reactions with calcium sulfate minerals, generating secondary polyhalite layers. Carnallite layers are mainly distributed in subbasins along fault zones in all three mining areas with small size. Ca-Cl-type waters rise to the surface along fault zones and mix with ground water as soon as they appear on the ground, forming the deposits of carnallite and bischofite after evaporation. During the generation of potassic salts, fault zones, on the one hand, control the margin of mining areas and the distribution of polyhalite layers. On the other hand, they act as the migration and reaction space for salt spring water, providing large amounts of ore-forming elements such as Ca<sup>2+</sup>, K<sup>+</sup>, and Mg<sup>2+</sup>. This study provides a theoretical basis for the exploration of potassium-rich brine in the Lop Nor Basin.

**Keywords:** Lop Nor Playa; carnallite; polyhalite; Ca-Cl brine; minerals distribution; fault zone

**Citation:** Wang, K.; Zhang, Y.; Han, J.; Ma, L.; Zheng, M.; Wu, Y.; Yang, B. Distribution and Genesis of Potassium-Bearing Minerals in Lop Nor Playa, Xinjiang, China. *Minerals* **2023**, *13*, 560. <https://doi.org/10.3390/min13040560>

Academic Editors: Paul Alexandre and Bimin Zhang

Received: 20 February 2023

Revised: 3 April 2023

Accepted: 12 April 2023

Published: 17 April 2023



**Copyright:** © 2023 by the authors. Licensee MDPI, Basel, Switzerland. This article is an open access article distributed under the terms and conditions of the Creative Commons Attribution (CC BY) license (<https://creativecommons.org/licenses/by/4.0/>).

## 1. Introduction

Potash fertilizer plays a very important role in crop growth. The balance between the supply and demand of fertilizer restricts the development of agriculture in a country [1]. China is a large agricultural country, but its dependence on foreign potash fertilizer is still over 50%, and 80% of this is imported from Russia, Belarus, Canada, and Israel [2].

Because of the special forming conditions of evaporite, global potash deposits are mainly distributed in closed basins in the 30–60° north latitude zone [1,3,4], such as the Saskatchewan Basin in Canada [5–8], Salt Range Basin in Pakistan [9–11], Sakon Nakhon Basin in Thailand [12–14], Delaware Basin in the USA [15], and some other basins in Europe [16–19]. In China, potassic salt is mostly produced from brines in the Qaidam Basin in Qinghai province [20–24] and Lop Nor Playa in the Tarim Basin [25–31]. In addition, minor production occurs in the Jiaghan Basin [32–34], Sichuan Basin [35–38], Simao Basin [39–42], and a few other basins [43–46]. Many studies have been carried out in the Lop Nor Playa and fruitful results have been achieved in relation to the geochemical characteristics of potassium-rich brines [31,43,47,48], tectonic evolution [49–51], sedimentary environment, and climate [28,29,31,52–54].

However, the total dissolved solids and content of potassium in brines in the mining areas have decreased due to intensive industrial exploitation of brine for more than 20 years [26]. In order to determine the relationship between the potassic salts and fault zones, geochemical research and X-ray powder diffraction were carried out over the past three years to determine the distribution characteristics and the genesis of the polyhalite ( $K_2Ca_2Mg(SO_4)_4 \cdot 2H_2O$ ) and carnallite ( $KMgCl_3 \cdot 6H_2O$ ) layers in the Lop Nor Playa. Our study provides a new direction for further exploitation of potassium-rich brines by dissolution and transformation of potassic salts in the Lop Nor Basin.

## 2. Geological Setting

The Lop Nor Playa is located in the easternmost part of the Tarim Basin (Figure 1) and belongs to the intersection of the Tarim Platform, Kunlun–Altun tectonic belt, and Beishan tectonic belt [49,50]. The Tarim Basin experienced several uplift periods during the Caledonian and Hercynian–Indosinian orogeny [55]. At that time, the depositional center of the Tarim Basin was situated westward of its present position. In the Neogene, due to the subduction of the Indian plate beneath the Eurasian plate, major faults around the basin became reactive. The Altun sinistral strike–slip fault and Kruktag dextral strike–slip fault produced a large displacement in this period, resulting in the Tarim Basin becoming a rhombic basin [56]. The Tibetan Plateau, Kunlun Mountains, and Altun Mountains were successively uplifted [57], and a large number of nappes were generated within the basin. At this time, the depositional center migrated progressively eastward and Lop Nor eventually became the depositional center.

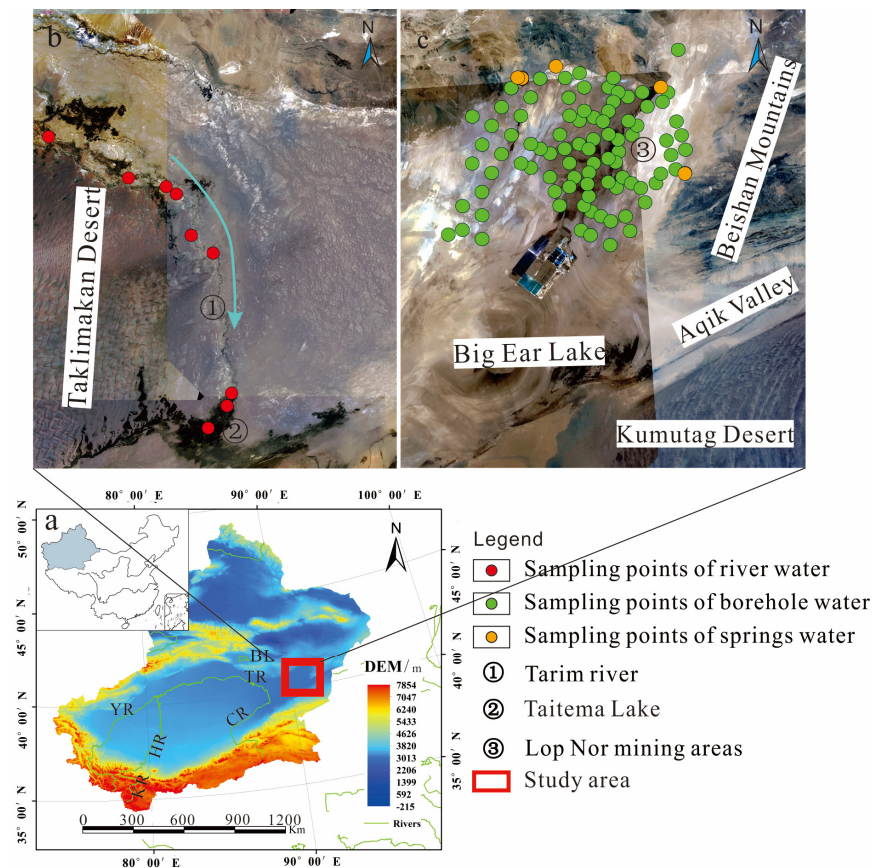


**Figure 1.** Location of the Lop Nor basin in China and the distribution of sampling points of this study; (a) shows the elevation of Xin Jiang Province and the approximate location of the Lop Nor Basin; (b) shows the sampling points along Tarim River; (c) shows the sampling points in the Lop Nor Basin. YR—Yarkand River; BL—Boston Lake; TR—Tarim River; CR—Cherchen River; HR—Hetian River. → shows the stream direction of Tarim River.

Due to the tectonic movements, the Lop Nor mining areas located in the northern part of the Lop Nor Playa became the lowest region of the whole basin. Because the northern part has the highest content of potassium and magnesium of the whole Lop Nor Playa, these areas are perfect for industrial exploitation. Faults developed in this area include the Kruktag Fault, Altun Faults, Kongque River Fault, and Cherchen Fault [58]. The Kruktag Fault controls the northern part of the Lop Nor Playa. It is a dextral strike-slip fault and is mainly controlled by two internal faults: the Xingdi Fault and Singur Fault [59]. The Altun Fault is a giant sinistral strike-slip fault, controlling the southern boundary of the Lop Nor Playa. In addition, due to the NEE-trending and near-EW-trending tectonic stresses [60], several faults developed in the mining areas (Figure 2). The Xinqing Platform and Luobei Depression are separated by the F4 fault, which is a normal fault with a strike of 30° and a dip of about 120°. The Luobei Depression and Tenglong Platform are separated by the F6 fault. The F4 and F6 faults generated the Luobei Depression. The F1 fault (Cherchen Fault) is a regional compressional and wrench fault. It passes through the Tenglong Platform and divides Tenglong into two parts. The F3 fault is located in the northern part of the mining area and represents its northern boundary [61]. Along the fault zone, there are a series of tectonic fissures, which become the migration paths of fissure water and pore water.

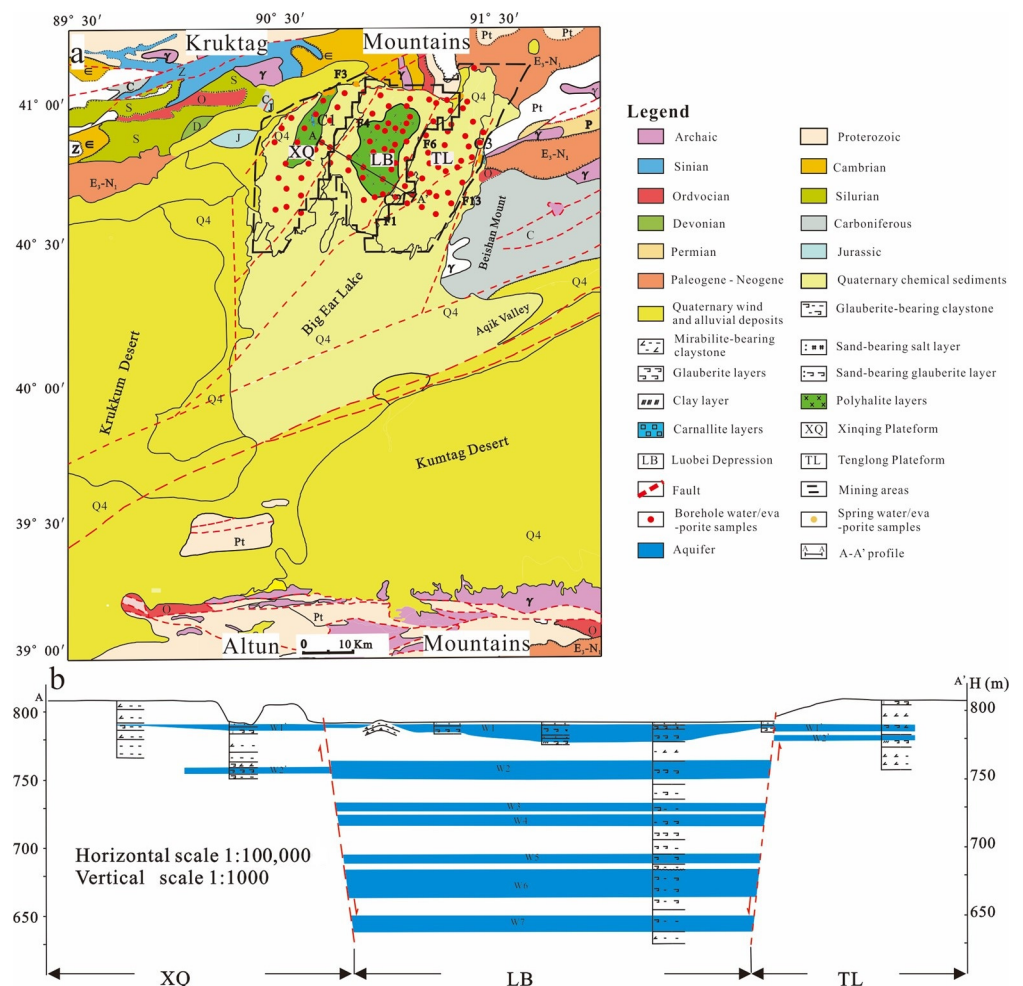


**Figure 2.** (a) Shows the simplified geological map of the Lop Nor basin [30,31,62–64]; (b) shows the cross-section of A-A' in the Lop Nor Basin. C1, C2, C3 are three deposits of carnallite layers.

The number of water reservoirs is varied in different mining areas because of the fault distribution. According to borehole data, there are seven brine layers in the Luobei Depression, including one phreatic layer and six confined water layers. There are two brine layers in the Xinqing Platform, both of which are confined water layers. There is one

phreatic layer and two confined water layers in the north of the Tenglong Platform, while only two confined water layers have developed in the south due to the influence of the F1 fault. According to a geological survey and remote sensing images, there are a large number of spring-point recharging mining areas along the faults. Spring water is another important source of brines developed in the Tarim Basin, in addition to rivers [62,65].

### 3. Sampling and Testing

#### 3.1. Sampling Methods

A total of 221 water samples and 256 evaporite samples were collected during a geological survey in the Lop Nor Playa. Water sampling points were mainly distributed along the Tarim River and boreholes, as well as fault zones around the mining areas, while mineral samples were mainly distributed around springs and boreholes in the mining areas.

Liquid samples were collected with 500 mL sampling bottles washed three times with water before sampling. Samples were collected in duplicate. After measuring the temperature, water density, and pH values of brines on site, each sample bottle was quickly sealed with tape to prevent evaporation and crystallization during storage. Because most evaporates deliquesce easily, evaporite samples were packed in a double-layer plastic-sealed bag after collection and kept sealed with minimum contact with air. Each sample was about 300–500 g.

#### 3.2. Analytical Methods

##### 3.2.1. X-ray Powder Diffraction

Evaporite samples were cleaned with ethyl alcohol and heated in an oven at 50 °C for 24 h. Then, samples were ground to 200 mesh. After drying, samples were sent to the Powder Crystal Laboratory of the Research Institute of China University of Geosciences (Beijing, China) for X-ray diffraction analysis. The measuring instrument was a Smart Lab 9 KW rotating anode ray diffractometer made by Rigaku, Japan. The anode was a Cu target, the scanning angle was 3°–70°, and the scanning step was 8°/min. MDI Jade 6.0 software was used for semi-quantitative analysis of the spectra.

##### 3.2.2. Major and Trace Elements Analysis

Impurities on the surface of evaporite samples were removed with ethyl alcohol and heating; then, samples were ground to 200 mesh. All collected liquid samples and solid samples were sent to the National Research Centre for Geoanalysis for major and trace element analysis. Major elements  $\text{Cl}^-$ ,  $\text{Na}^+$ ,  $\text{K}^+$ ,  $\text{SO}_4^{2-}$ ,  $\text{Mg}^{2+}$ ,  $\text{Ca}^{2+}$ ,  $\text{CO}_3^{2-}$ , and  $\text{HCO}_3^-$  and trace elements  $\text{Li}^+$ ,  $\text{B}^{3+}$ ,  $\text{Br}^-$ ,  $\text{I}^-$ ,  $\text{Rb}^+$ ,  $\text{Cs}^+$ , and  $\text{Sr}^{2+}$ , as well as  $\text{NO}_3^-$ , were determined in liquid samples.  $\text{Na}^+$ ,  $\text{K}^+$ ,  $\text{Mg}^{2+}$ ,  $\text{Ca}^{2+}$ , and  $\text{B}^{3+}$  were quantified using an inductively coupled plasma atomic emission spectrometer (PE8300). The analytical error was less than 0.2% for  $\text{Ca}^{2+}$  and  $\text{Mg}^{2+}$ , less than 0.5% for  $\text{Na}^+$  and  $\text{K}^+$ , and less than 1% for  $\text{B}^{3+}$ .  $\text{Li}^+$ ,  $\text{Br}^-$ ,  $\text{I}^-$ ,  $\text{Rb}^+$ ,  $\text{Cs}^+$ , and  $\text{Sr}^{2+}$  were detected using a plasma mass spectrometer (PE300Q). The analytical error was less than 2%.  $\text{Cl}^-$ ,  $\text{CO}_3^{2-}$ ,  $\text{HCO}_3^-$ ,  $\text{NO}_3^-$ , and  $\text{SO}_4^{2-}$  were measured through ion chromatography, and the analytical error was less than 0.2%. The pH value was measured using a Hana HI9126 portable pH acidity meter, and the error was less than 1%. Brine density was measured at day temperature in Lop Nor using a DMA35 portable densitometer with a measuring accuracy better than 0.1%.

## 4. Results

### 4.1. X-ray Powder Diffraction Analysis

There is a large amount of evaporite minerals on the surfaces of Lop Nor mining areas. Due to the different ion contents in the three mining areas, there are many differences in the minerals in different areas (Figure 3, Table 1).

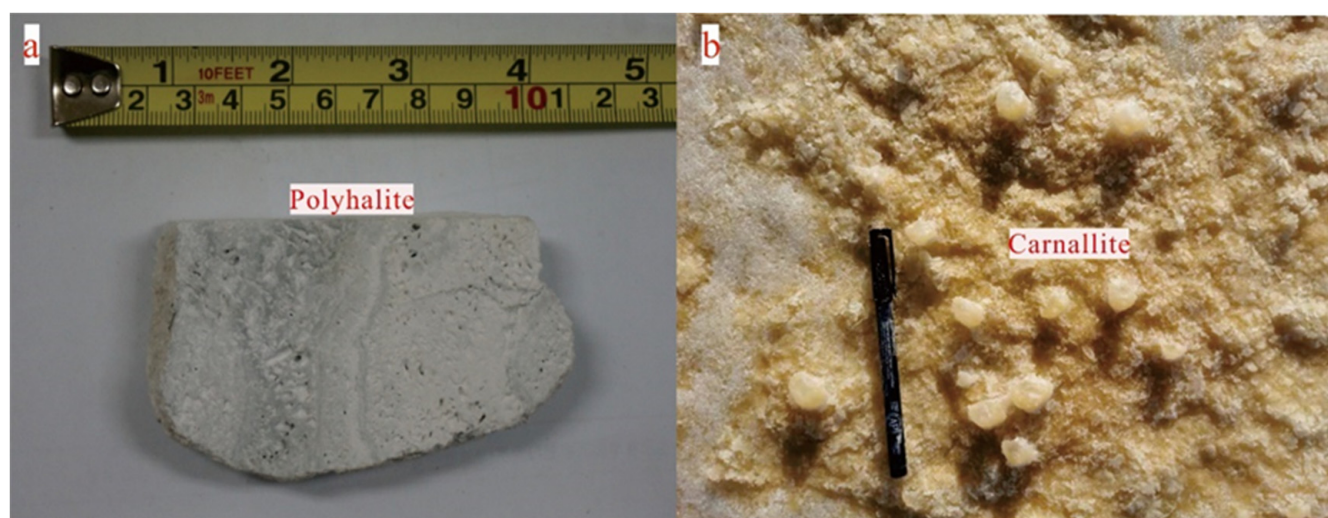


**Figure 3.** Pictures of polyhalite and carnallite; (a) polyhalite, sampled in the north of the Luobei Depression; (b) carnallite, sampled in the east part of the Tenglong Platform.

**Table 1.** Results of X-ray Diffraction of samples.

Mineral	Number *	Distribution Areas
Gypsum	53 *	Tenglong mining area; Luobei Mining area; Xinqing mining area
Halite	492 *	Tenglong mining area; Luobei Mining area; Xinqing mining area
Bischofite	4	Tenglong Mining area
Carnallite	5	Tenglong Mining area; Luobei mining area; Xinqing mining area
Nitrate	1	Tenglong mining area
Magnesite	372 *	Luobei mining area; Xinqing mining area
Polyhalite	5	Xinqing mining area; Luobei mining area

\* Data are derived from this study results and reference [63,64].

As the Luobei Depression is the concentration center of the Lop Nor Basin, there are large amounts of minerals on the surface of the Luobei, such as gypsum ( $\text{CaSO}_4 \cdot 2\text{H}_2\text{O}$ ), mirabilite ( $\text{Na}_2\text{SO}_4 \cdot 10\text{H}_2\text{O}$ ), and glauberite ( $\text{Na}_2\text{SO}_4 \cdot \text{CaSO}_4$ ) (Figure 2). From the east and west sides to the middle, evaporite minerals gradually evolve from gypsum and glauberite to halite ( $\text{NaCl}$ ) layers. On top of the gypsum and anhydrite ( $\text{CaSO}_4$ ) layer, there is a thin layer of polyhalite ( $\text{K}_2\text{Ca}_2\text{Mg}(\text{SO}_4)_4 \cdot 2\text{H}_2\text{O}$ ) (Figure 4a), which is located between the F4 and F6 fault zones. The polyhalite layer is consistent with the long axis of the strike of the Luobei Depression. On the surface of the Xinqing Platform, there are mainly gypsum layers. However, halite layers are distributed along fault zones in the east of the Xinqing Platform and a polyhalite layer (Figure 4b) occurs in the Xianche spring, which is in agreement with Li Boyun's [64] findings. Since the Tenglong Platform is located at the junction of the Lop Nor mining area and Beishan, the fault structures are extremely developed. In addition to a large variety of glauberite, gypsum, and other minerals on the surface of the Tenglong Platform, there is a halite layer near the F4 fault and carnallite ( $\text{KMgCl}_3 \cdot 6\text{H}_2\text{O}$ ) and bischofite ( $\text{MgCl}_2 \cdot 6\text{H}_2\text{O}$ ) layer along the F13 fault zone (Figure 2(C3)), while in the middle and eastern parts, glauberite and other minerals are distributed. Moreover, carnallite and bischofite deposits are distributed in the secondary depressions around the fault zone (Figure 2(C3)). Meanwhile, there are thin layers of carnallite that have developed in the Xinqing Platform (C1) and Luobei Depression (C2), both of which are located along fault zones.

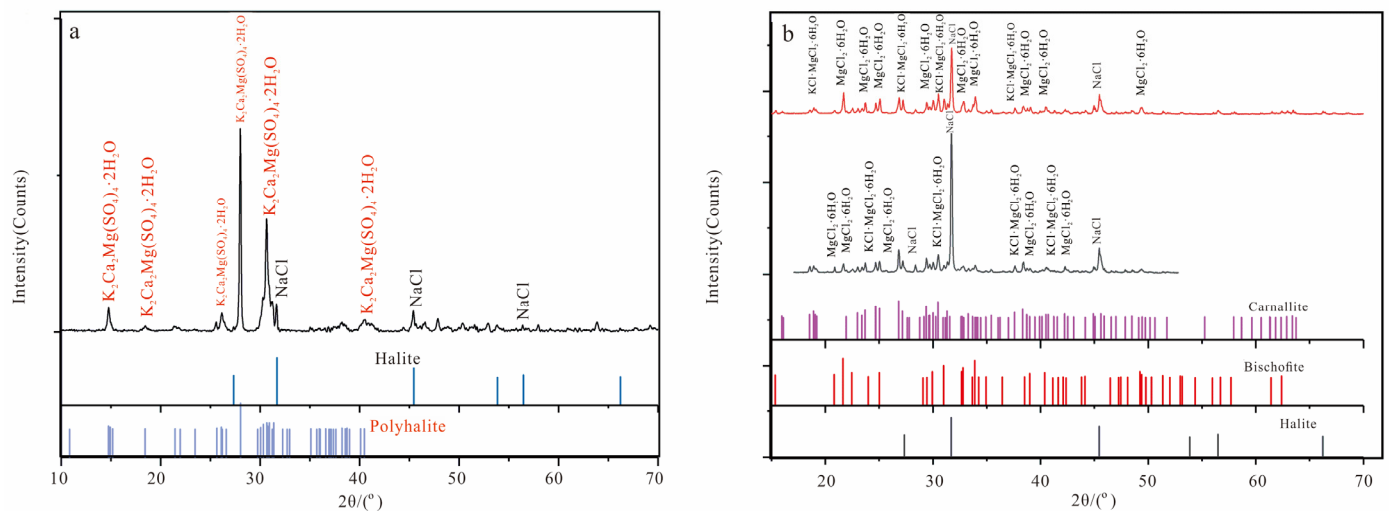


**Figure 4.** XRD patterns of carnallite and polyhalite; (a) patterns of polyhalite and halite in the Lop Nor basin, (b) patterns of carnallite bischofite and halite in the Lop Nor basin.

#### 4.2. Characteristics of Geochemistry

By plotting all the collected liquid samples on a Piper diagram (Figure 5), it was found that most liquid samples such as borehole brine, spring water, and underground water have the same geochemistry characteristics. The waters collected in the Lop Nor mining areas are mainly Na-Cl-SO<sub>4</sub> type. The main cation is Na<sup>+</sup>, which accounted for about 80%–95%, and the second is Mg<sup>2+</sup>, accounting for about 5%–20%. Ca<sup>2+</sup> is a minor cation, representing less than 5%. Meanwhile, Cl<sup>−</sup> is the main anion, accounting for about 80%–90%, and about 10%–20% is SO<sub>4</sub><sup>2−</sup>. However, spring water located near the F13 fault zone in the eastern part of the Tenglong Platform has a different composition to those in the mining areas. It is a Mg-Cl-type water, and its main cation is Mg<sup>2+</sup>, accounting for about 95%, with very little Na<sup>+</sup>, K<sup>+</sup>, or Ca<sup>2+</sup>. The main anion in this water is Cl<sup>−</sup>, accounting for about 99%, indicating another recharge to mining areas.

In contrast to those in the Lop Nor Basin, the water geochemistry characteristics of the Tarim River are related to sampling points, especially in the low reaches of the Tarim River, where Na<sup>+</sup>, K<sup>+</sup>, and Mg<sup>2+</sup> increase downstream [62]. The water composition near Taitema Lake (orange circles in Figure 5) is similar to that in the Lop Nor Basin; the water in those areas is all Na-SO<sub>4</sub>-type water, and Taitema water has a high content of Na<sup>+</sup>, at about 70%, as well as a high Ca<sup>2+</sup> content, which is much higher than the content found in mining areas. The main anions are CO<sub>3</sub><sup>2−</sup> and HCO<sub>3</sub><sup>−</sup>, accounting for about 30%–50%, and they have similar contents of SO<sub>4</sub><sup>2−</sup> and Cl<sup>−</sup>, accounting for about 25%–30%.

The distributions (Figure 6) of K<sup>+</sup>, Mg<sup>2+</sup>, and Cl<sup>−</sup> in the mining areas are quite consistent. The highest values for these three ions are mainly concentrated in the middle of the Luobei Depression. Ion content shows a decreasing trend from the Luobei Depression to the other two platforms, but high values of ions appear near fault zones, indicating that there are high-salinity brines recharging to mining areas along fault zones. However, the distribution of Ca<sup>2+</sup> is different. The content of Ca<sup>2+</sup> in the water is lower than 0.25 g/L, and the highest value appears near the F4 and F6 faults. As brines in the mining areas have a low Ca<sup>2+</sup> content, there may be deep water supply to mining areas along faults.

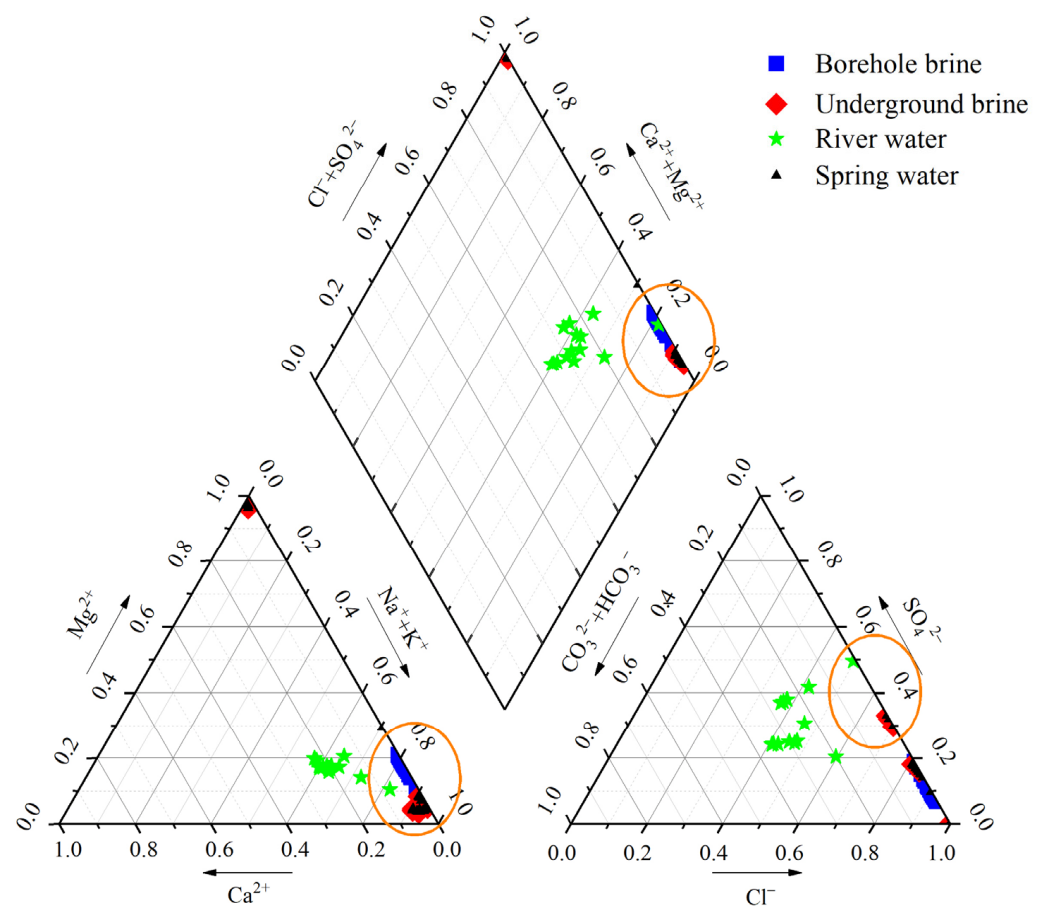


Figure 5. Piper triangle phase diagram of inflow waters of the Lop Nor Basin.

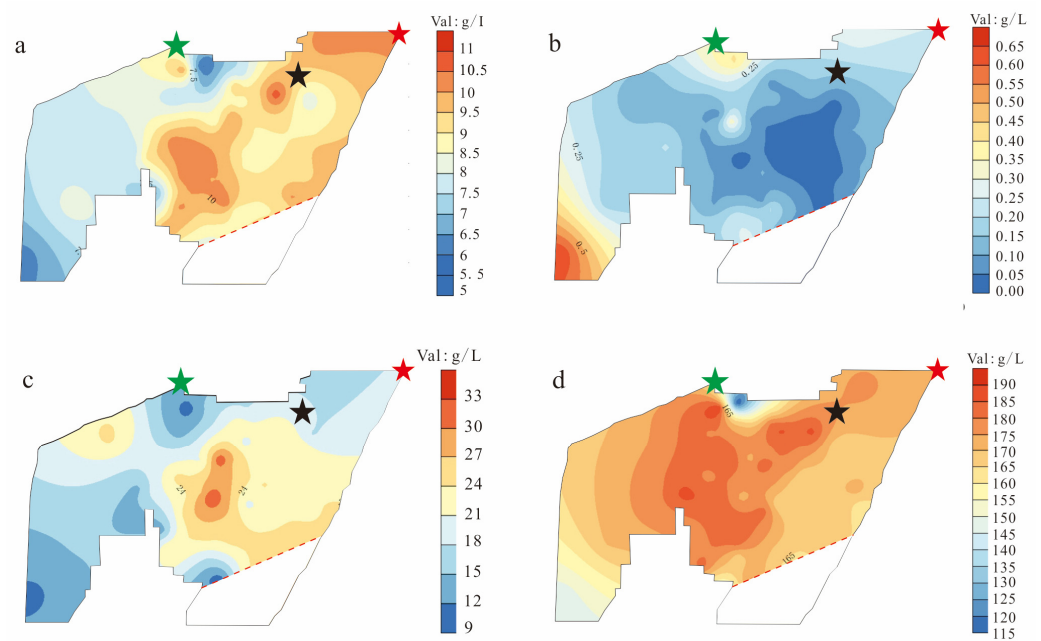


Figure 6. Distribution of  $K^+$ ,  $Ca^{2+}$ ,  $Mg^{2+}$ , and  $Cl^-$  in Lop Nor mining areas; (a) shows the distribution of  $K^+$ , (b) shows the distribution of  $Ca^{2+}$ , (c) shows the distribution of  $Mg^{2+}$ , and (d) shows the distribution of  $Cl^-$  in the Lop Nor Playa. The coordinates of  $\star$  are  $90^\circ53'05''$  E,  $41^\circ06'03''$  N, the coordinates of  $\blackstar$  are  $91^\circ15'05''$  E,  $41^\circ03'36''$  N, the coordinates of  $\color{red}\star$  are  $91^\circ37'04''$  E,  $41^\circ10'03''$  N [66] (Testing results of water samples are shown in Appendix A below).

## 5. Discussion

### 5.1. Genesis of Carnallite in Lop Nor Basin

Carnallite is one of the last minerals to be formed through brine evaporation according to recent models [48,67]. Previous studies have shown that deep source water recharge plays an important role in the formation of carnallite [67–69]. When deep water mixes with meteoric waters in different proportions, it forms different water types. When the meteoric/deep source water proportion is above 83:1, the meteoric water will turn into Na-HCO<sub>3</sub>-Cl-type water. When this proportion is below 40:1, the resulting brines turn into Ca-Cl-type water. When the proportion is between 40:1 and 83:1, the mixing water will turn into the Cl-SO<sub>4</sub> type [48,67,68].

Carnallite is mainly distributed in the subbasin near the regional fault zone in the Xinqing Platform, Luobei Depression, and eastern part of the Tenglong Platform (Figure 2) based on XRD results and former studies [64]. Many spring points are distributed along fault zones, most of which provide seasonal supply to the Lop Nor Basin. Chemical analysis results show that the water of springs in the east of the Tenglong Platform is Ca-Cl-type water, while the water type of boreholes is Cl-SO<sub>4</sub>-type water, indicating a great difference in Ca<sup>2+</sup> content between these two water bodies. Meanwhile, water along the fault zones in the eastern part of the Tenglong Platform in Figure 7 falls at the junction of the carnallite and bischofite stability field, indicating that the waters along fault zones have entered the late stage of brine evaporation, then gradually form carnallite layers.

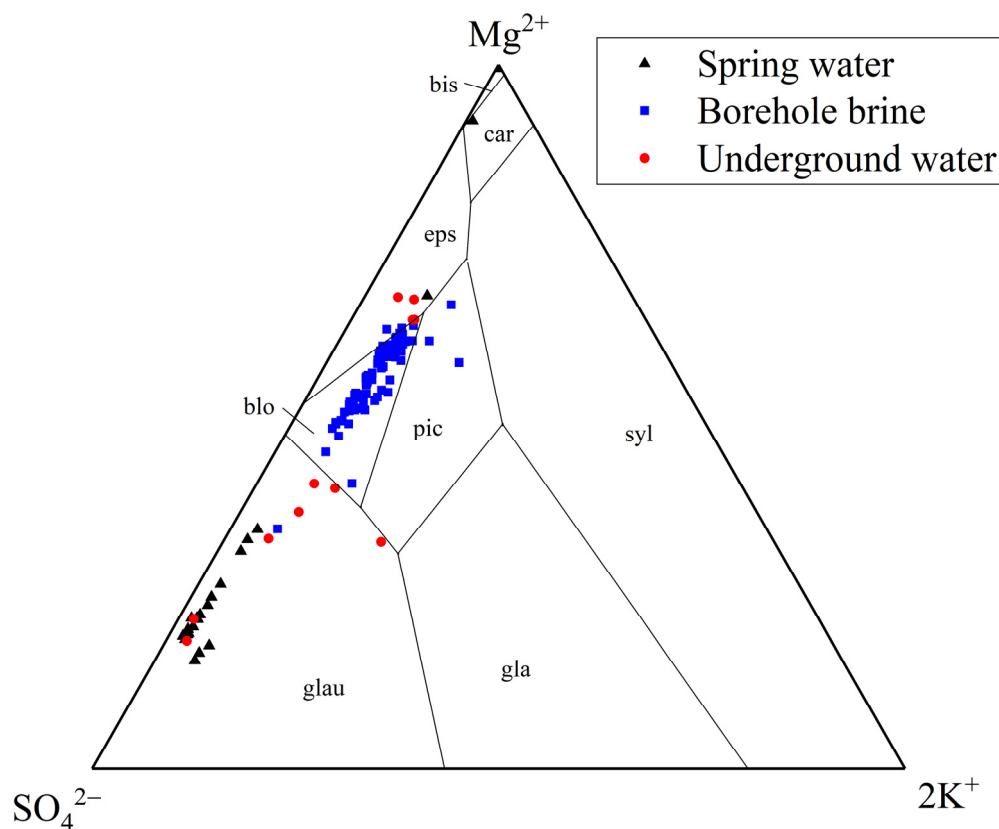


**Figure 7.** The phase diagram of Na<sup>+</sup>, K<sup>+</sup>, Mg<sup>2+</sup> // Cl<sup>-</sup>, SO<sub>4</sub><sup>2-</sup>-H<sub>2</sub>O five-element water-element system in the Lop Nor Basin at 25 °C; bis, bischofite; car, carnallite; eps, epsomite; blo, bloedite; pic, picromerite; syl, sylvite; gla, glauberite; glau, glauber salt.

As the terminal lake of the Tarim Basin, Lop Nor accepts all inflow waters of the Tarim Basin, such as the Tarim River, Kongque River, and Cherchen River [31,62], as well as salt spring water that rises along fault zones. Waters migrate from Big Ear Lake and rivers to mining areas through fractures and faults. Strong evaporation occurs during the migration

process, the salinity of water increases, and this concentration will continue even after arriving in mining areas. Moreover, when migrating through channels of fractures and faults, water from deep underground reacts with the surrounding rocks and carries a large number of ore-forming materials such as  $\text{Ca}^{2+}$ ,  $\text{K}^+$ ,  $\text{Mg}^{2+}$ ,  $\text{Na}^+$ , and  $\text{Cl}^-$ . Therefore, the water type changes from Na-Cl- $\text{SO}_4$  to Ca-Cl upon mixing with brines in the Lop Nor Basin. During this process, the calcium content first increases and then decreases because of the precipitation of carbonate and sulfate (Figure 8b). Halite begins to occur at the end of the calcite stage.  $\text{K}^+$  and  $\text{Cl}^-$  combine after the depletion of  $\text{Ca}^{2+}$  and  $\text{Na}^+$ , and sylvite begins to be generated but is replaced by carnallite after reacting with high-salinity brines. For these reasons, sylvite rarely occurs in natural environments. At the end of the process, magnesium combines with chloride to produce bischofite; however, carnallite and bischofite usually occur along fault zones, where deep waters rise to the surface.

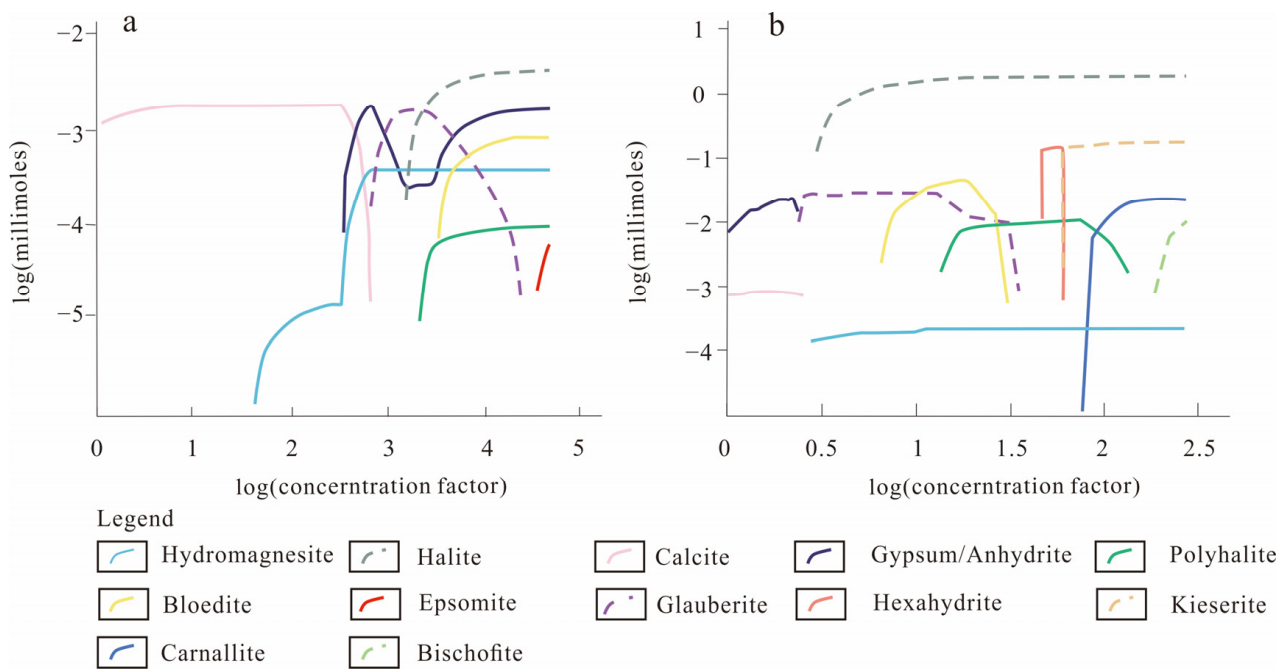


**Figure 8.** Modeling of Tarim water and brine evolution pathway in the Lop Nor Basin by EQL/EVP program in closed system conditions at 25 °C and  $P_{\text{CO}_2}$  of  $10^{-3.4}$ . (a) Simulated evolution of Tarim river water; (b) simulated evolution of brines at the edge of the Lop Nor basin [48].

### 5.2. Genesis of Polyhalite in Lop Nor Basin

Previous studies on the formation of polyhalite [70–77] showed that when brines with high contents of potassium and magnesium encounter a large amount of calcite or gypsum deposits, there will be a metasomatic reaction between the minerals and brines. As a result, secondary polyhalite begins to replace calcite. Ayora [78] and Rahimpour [73] assumed that because of the  $\text{SO}_4^{2-}$  depletion observed during the evaporation process, it is difficult to form primary polyhalite. However, according to previous studies [79–83], there may be primary polyhalite at an early stage of diagenesis without the involvement of concentrated brines. Studies on polyhalite in the Sichuan Basin and Qarhan Salt Lake [38,84–86] showed that polyhalite layers are the result of reactions between sulfate minerals and brines carrying potassium and magnesium.

There are several polyhalite layers and large amounts of calcite and gypsum as well as glauberite in the central Xinqing Platform and central Luobei Depression (Table 1 and Figure 2). Brines around evaporites have values of total dissolved solids ranging from 280 g/L to 370 g/L. Plotting points in Figure 5 show that the brines near where polyhalite was sampled are Na-Cl- $\text{SO}_4$ -type water, which has little calcium, so the calcium in polyhalite comes from a different source.

As the Luobei Depression is the lowest subbasin of the Lop Nor Playa, brines from the whole Lop Nor basin will migrate to the Luobei through fractures. At the beginning of the evaporation of Tarim River water (Figure 8a), large amounts of  $\text{Ca}^{2+}$  are depleted, and calcite and gypsum were generated on the surface of the Lop Nor Playa. During the process of evaporation, residual  $\text{Ca}^{2+}$  is combined with  $\text{Na}^+$  and  $\text{SO}_4^{2-}$ , producing glauberite during the process of halite generation. When the content of glauberite reaches its peak, glauberite turns into polyhalite, as there is a reaction between glauberite and  $\text{K}^+$  and  $\text{Mg}^{2+}$  in brines. Because the reaction takes time, the polyhalite layer usually generates at a distance from the fault zones.

## 6. Conclusions

Lop Nor is the terminal depression of the Tarim Basin, where a potassium-rich brine exists after concentration and abundant evaporation minerals are formed. The content of  $\text{K}^+$  in brines has decreased a lot after 20 years of exploitation. We can draw several conclusions based on the results of the geochemistry analysis of the brines and X-ray powder diffraction of salts:

1. Large amounts of potassium-rich minerals exist in the Lop Nor Basin. There are polyhalite layers in the Luobei Depression and in the central–east part of the Xin-qing Platform. Carnallite layers are mainly distributed along fault zones. It can relieve the short-supply status of potassium by dissolution and transformation of the potassic salts.
2. On one hand, large-scale faults control the margin of mining areas as well as the distribution of ore beds. On the other hand, fault zones provide channels for the migration of brines. When brines rise up through faults, there is a reaction between the water and wall rock, so fluids become enriched with ions such as  $\text{Ca}^{2+}$ ,  $\text{K}^+$ , and  $\text{Mg}^{2+}$ .
3. Waters from deep underground rise and reach mining areas along fault zones. When Ca-Cl-type brines mix with ground water, carnallite and bischofite begin to form. Polyhalite, on the other hand, is an inevitable result of the water evolution process for sulfate-type water. When brines with high contents of potassium and magnesium reach a depression where there are gypsum or glauberite layers, the potassium and magnesium react with these minerals and change them into polyhalite.

**Author Contributions:** L.M. and M.Z. designed the research in the manuscript. K.W. and Y.Z. participated in sample collection. K.W. wrote the first draft and prepared all figures. J.H., Y.W. and B.Y. drew Figures 4 and 8. L.M. and K.W. wrote the first draft and prepared all figures. All authors have read and agreed to the published version of the manuscript.

**Funding:** This work was funded by the subject of China Geological Survey project (No.DD20230037, No. DD20160054) and Central Public Interest Scientific Institution Basal Research Fund (No. JYYWF2018).

**Data Availability Statement:** Correspondence and requests for materials should be addressed to L.M.

**Acknowledgments:** We are grateful to Wenxue Li and Baocheng Ma from SDIC Xinjiang Lop Nor Potash Co., Ltd. for their help with field work, and Zihong Zhu from the Institute of Subtropical Agriculture, CAS, and Wei Chen from the School of Land Science and Technology, CUGB, for their suggestions on figures.

**Conflicts of Interest:** The authors declare no competing interest.

## Appendix A. Geochemical Results of Water Samples in the Lop Nor Basin

Sample	TDS	Na <sup>+</sup>	K <sup>+</sup>	Ca <sup>2+</sup>	Mg <sup>2+</sup>	Cl <sup>-</sup>	SO <sub>4</sub> <sup>2-</sup>	HCO <sub>3</sub> <sup>-</sup>	CO <sub>3</sub> <sup>2-</sup>	Li	B	Br	I	Rb	Cs	Sr
				g/L						mg/L						
1	4.78	1.06	0.05	0.29	0.18	1.46	1.62	120.00	0.00	0.45	4.90	<0.2	<0.01	0.02	<0.01	10.00
2	0.64	0.10	0.01	0.06	0.03	0.13	0.19	132.00	0.00	0.05	0.23	0.03	0.00	0.00	<0.001	1.35
3	0.60	0.08	0.01	0.06	0.03	0.11	0.17	148.00	0.00	0.05	0.22	0.03	0.00	0.00	<0.001	1.22
4	0.62	0.09	0.01	0.06	0.03	0.12	0.18	137.00	0.00	0.05	0.23	0.03	0.00	0.00	<0.001	1.32
5	0.69	0.11	0.01	0.05	0.03	0.14	0.20	148.00	0.00	0.05	0.22	0.03	0.00	0.00	<0.001	1.39
6	1.00	0.15	0.02	0.09	0.04	0.19	0.34	163.00	0.00	0.05	0.31	0.04	0.00	0.00	<0.001	2.36
7	0.99	0.20	0.01	0.07	0.04	0.27	0.25	155.00	0.00	0.06	0.29	0.05	0.01	0.00	<0.001	1.78
8	1.36	0.30	0.02	0.12	0.10	0.36	0.46	0.41	0.00	0.06	0.41	0.09	0.02	0.00	<0.05	2.27
9	0.57	0.10	0.01	0.07	0.04	0.14	0.21	0.15	0.00	0.03	0.13	0.04	0.00	0.00	<0.05	1.19
10	0.60	0.12	0.01	0.07	0.04	0.14	0.23	0.15	0.00	0.04	0.16	0.04	0.00	0.00	<0.05	1.24
11	0.58	0.10	0.01	0.08	0.04	0.14	0.22	0.17	0.00	0.03	0.19	0.04	0.00	0.00	<0.05	1.24
12	0.82	0.15	0.01	0.09	0.04	0.21	0.31	0.14	0.00	0.05	0.36	0.04	0.00	0.00	<0.05	1.72
13	17.20	4.52	0.23	0.75	0.62	6.07	5.01	0.15	0.00	1.92	20.80	0.62	0.01	0.07	<0.5	24.20
14	366.80	75.70	13.50	0.10	36.50	186.00	54.70	219.00	86.70	24.60	101.00	25.50	<1	2.07	<1	<1
15	488.01	1.52	1.11	4.55	125.00	354.00	1.35	263.00	215.00	141.00	<10	<20	<1	<1	<1	71.30
16	96.86	29.90	0.81	0.56	2.82	40.20	22.40	145.00	20.00	1.81	21.50	<5	0.76	0.37	<0.025	21.60
17	96.22	30.50	0.74	0.60	2.46	40.70	21.10	84.20	37.10	1.44	13.90	<5	0.71	0.29	<0.025	15.30
18	28.03	8.60	0.11	0.73	0.46	11.30	6.65	180.00	0.00	0.59	3.91	1.35	0.17	0.06	<0.005	13.00
19	25.26	7.95	0.12	0.72	0.38	9.88	6.02	189.00	0.00	0.49	3.59	1.13	0.14	0.05	<0.0025	12.60
20	30.56	9.67	0.13	0.68	0.43	12.20	7.25	200.00	0.00	0.45	3.35	<1	0.14	0.06	<0.005	9.75
21	363.67	96.30	9.69	0.12	23.80	184.00	49.60	163.00	0.00	24.50	84.50	<20	<1	1.62	<1	3.59
22	366.40	97.30	10.40	0.12	24.00	185.00	49.40	177.00	0.00	25.20	93.30	<20	<1	1.70	<1	3.53
23	367.01	96.60	10.10	0.09	23.80	181.00	55.20	211.00	0.00	24.60	91.90	<20	<1	1.65	<1	3.42
24	329.04	92.60	9.20	0.24	18.20	167.00	41.50	304.00	0.00	17.90	67.70	<20	<1	1.54	<1	4.67
25	344.61	106.00	6.79	0.15	13.20	176.00	42.40	69.10	0.00	12.90	63.60	<20	<1	1.08	<1	5.67
26	339.09	102.00	7.57	0.16	14.30	178.00	37.00	61.50	0.00	14.70	59.70	<20	<1	1.31	<1	4.94
27	381.11	95.60	9.61	0.03	26.30	159.00	90.50	76.70	0.00	20.30	86.60	26.70	<1	1.39	<1	1.54
28	352.34	110.00	8.39	0.18	14.30	180.00	39.40	73.50	0.00	15.10	60.60	<20	1.37	1.24	<1	8.13
29	357.12	96.90	8.24	0.12	22.80	181.00	48.00	64.60	0.00	22.60	81.70	21.20	1.17	1.41	<1	3.60
30	337.90	93.00	7.78	0.14	20.20	159.00	57.70	82.40	0.00	13.40	61.90	<20	1.16	1.12	<1	5.38
31	362.67	95.60	9.70	0.18	25.10	181.00	50.90	185.00	0.00	26.00	93.00	<20	1.02	1.64	<1	3.02
32	368.72	96.50	10.20	0.10	25.70	184.00	52.00	221.00	0.00	22.70	100.00	20.20	<1	1.74	<1	3.10
33	374.68	102.00	10.30	0.09	24.90	175.00	62.20	195.00	0.00	24.30	88.60	22.60	<1	1.75	<1	2.42
34	351.53	90.10	8.64	0.21	24.00	170.00	58.50	84.90	0.00	17.70	73.40	23.70	<1	1.59	<1	2.29
35	352.97	94.80	10.10	0.13	24.20	179.00	44.60	144.00	0.00	23.40	92.00	<20	<1	1.68	<1	3.00
36	356.29	103.00	9.18	0.15	19.00	187.00	37.80	155.00	0.00	18.80	76.10	<20	<1	1.52	<1	4.73
37	352.37	109.00	7.55	0.21	14.40	181.00	40.10	108.00	0.00	14.40	52.10	<20	<1	1.18	<1	4.54
38	393.08	96.30	9.57	0.04	27.10	160.00	100.00	74.10	0.00	21.20	87.90	27.30	<1	1.49	<1	<1

Sample	TDS	Na <sup>+</sup>	K <sup>+</sup>	Ca <sup>2+</sup>	Mg <sup>2+</sup>	Cl <sup>-</sup>	SO <sub>4</sub> <sup>2-</sup>	HCO <sub>3</sub> <sup>-</sup>	CO <sub>3</sub> <sup>2-</sup>	Li	B	Br	I	Rb	Cs	Sr
				g/L						mg/L						
39	356.80	98.30	8.04	0.11	21.90	176.00	52.40	54.50	0.00	15.20	65.90	21.00	<1	1.16	<1	2.18
40	359.60	98.20	8.23	0.10	23.90	170.00	59.10	68.40	0.00	16.50	81.00	23.30	1.18	1.29	<1	2.06
41	355.07	119.00	8.15	0.28	8.68	178.00	40.90	64.00	0.00	12.40	44.50	<20	<1	1.25	<1	3.48
42	362.18	105.00	9.28	0.11	18.90	168.00	60.70	188.00	0.00	17.70	71.40	<20	<1	1.50	<1	3.21
43	354.94	94.60	8.34	0.15	23.60	176.00	52.20	51.30	0.00	15.10	68.20	21.60	<1	1.19	<1	2.80
44	351.03	93.90	8.15	0.21	23.60	160.00	65.10	67.80	0.00	16.00	68.90	21.20	<1	1.22	<1	2.49
45	359.11	89.50	8.95	0.09	25.60	165.00	69.90	68.40	0.00	18.80	81.60	23.50	<1	1.39	<1	1.59
46	354.98	91.10	8.71	0.11	24.20	170.00	60.80	58.90	0.00	16.90	59.70	24.10	<1	1.19	<1	2.43
47	356.20	92.20	8.32	0.08	23.00	157.00	75.50	101.00	0.00	15.60	76.10	21.50	<1	1.27	<1	2.67
48	369.42	93.40	9.97	0.06	27.50	181.00	57.30	190.00	0.00	27.00	92.10	20.60	1.12	1.76	<1	2.05
49	364.19	98.90	10.10	0.09	22.90	185.00	47.00	198.00	0.00	21.40	88.60	<20	<1	1.64	<1	2.51
50	371.20	102.00	9.34	0.06	21.50	167.00	71.20	96.30	0.00	17.00	68.20	<20	<1	2.17	<1	2.72
51	359.69	87.80	9.31	0.09	28.20	169.00	65.20	90.60	0.00	18.90	85.50	31.60	1.81	1.47	<1	2.57
52	384.12	96.60	9.55	0.02	27.10	163.00	87.80	54.50	0.00	19.90	91.30	29.40	1.62	1.47	<1	2.00
53	359.47	101.00	10.10	0.17	21.60	183.00	43.40	199.00	0.00	20.00	70.00	<20	<1	1.73	<1	3.90
54	357.49	106.00	8.77	0.17	19.00	182.00	41.50	47.50	0.00	20.70	77.90	<20	<1	1.53	<1	2.85
55	359.24	94.30	9.00	0.13	24.50	166.00	65.30	7.60	0.00	13.90	68.30	21.80	1.13	1.30	<1	4.38
56	377.06	85.20	10.30	0.03	33.00	173.00	75.30	233.00	0.00	28.40	104.00	23.80	<1	2.00	<1	<1
57	370.31	97.60	9.87	0.11	25.80	182.00	54.70	233.00	0.00	25.30	96.10	23.20	<1	1.78	<1	3.12
58	369.57	94.60	10.30	0.07	26.30	179.00	59.10	199.00	0.00	23.30	93.40	21.10	<1	1.80	<1	1.42
59	358.14	93.40	10.20	0.09	25.00	178.00	51.20	245.00	0.00	25.10	111.00	<20	<1	1.71	<1	3.55
60	372.24	100.00	9.02	0.04	24.30	170.00	68.80	82.40	0.00	17.50	86.10	25.80	1.59	1.39	<1	2.02
61	373.07	101.00	7.96	0.02	24.40	181.00	58.60	88.10	0.00	17.30	87.80	21.60	<1	1.37	<1	2.33
62	357.52	94.40	8.05	0.11	24.70	173.00	57.20	59.60	0.00	16.30	74.50	23.20	<1	1.29	<1	2.06
63	354.94	107.00	7.36	0.14	13.30	133.00	94.00	136.00	0.00	12.40	40.90	<20	<1	1.16	<1	4.60
64	358.07	92.60	8.30	0.11	23.70	160.00	73.30	64.00	0.00	17.20	76.10	21.30	<1	1.29	<1	2.94
65	296.79	84.10	6.50	0.23	17.20	140.00	48.70	62.10	0.00	10.70	57.30	<20	<1	<1	<1	6.38
66	363.07	93.80	9.83	0.11	25.30	183.00	50.80	228.00	0.00	24.00	95.30	<20	<1	1.77	<1	4.06
67	395.66	115.00	8.97	0.01	20.00	165.00	86.60	74.10	0.00	20.00	88.00	<20	<1	1.36	<1	1.26
68	387.18	100.00	10.10	0.03	25.70	168.00	83.30	55.80	0.00	18.50	93.20	24.30	<1	1.55	<1	<1
69	343.74	102.00	8.33	0.17	15.60	171.00	46.60	41.80	0.00	11.80	49.60	<20	<1	1.16	<1	2.82
70	359.71	97.10	9.66	0.15	22.40	184.00	46.20	200.00	0.00	23.60	84.10	<20	1.14	1.68	<1	5.88
71	379.79	102.00	8.96	0.04	23.30	173.00	72.40	91.90	0.00	23.30	95.80	20.70	1.33	1.51	<1	3.39
72	362.78	101.00	9.42	0.35	20.90	183.00	47.90	205.00	0.00	19.60	82.70	<20	<1	1.50	<1	4.62
73	358.71	101.00	8.95	0.08	20.50	185.00	43.00	180.00	0.00	18.80	79.00	<20	<1	1.40	<1	4.08
74	378.33	99.10	9.87	0.10	25.20	166.00	78.00	63.40	0.00	18.30	87.10	24.20	<1	1.43	<1	1.54
75	356.21	94.60	7.68	0.15	24.10	173.00	56.60	75.40	0.00	15.70	76.60	21.20	<1	1.16	<1	2.63
76	343.13	91.10	8.22	0.14	23.20	175.00	45.40	69.10	0.00	13.80	51.20	20.40	<1	1.14	<1	4.70
77	372.09	96.70	9.91	0.06	27.20	183.00	55.00	224.00	0.00	24.40	93.30	21.00	1.54	1.72	<1	3.79
78	369.78	86.80	8.62	0.10	32.70	173.00	68.30	263.00	0.00	26.70	122.00	25.90	<1	1.77	<1	2.19
79	402.60	109.00	8.84	0.01	24.40	167.00	93.30	48.20	0.00	20.40	78.10	<20	<1	1.38	<1	1.11

Sample	TDS	Na <sup>+</sup>	K <sup>+</sup>	Ca <sup>2+</sup>	Mg <sup>2+</sup>	Cl <sup>-</sup>	SO <sub>4</sub> <sup>2-</sup>	HCO <sub>3</sub> <sup>-</sup>	CO <sub>3</sub> <sup>2-</sup>	Li	B	Br	I	Rb	Cs	Sr
		g/L								mg/L						
80	395.98	109.00	8.33	0.03	22.80	171.00	84.70	125.00	0.00	18.90	65.30	<20	<1	1.28	<1	1.15
81	352.60	112.00	7.36	0.16	13.80	179.00	40.20	75.40	0.00	13.10	56.10	<20	<1	1.12	<1	4.85
82	381.03	106.00	9.22	0.04	22.70	168.00	75.00	64.00	0.00	15.30	82.00	<20	<1	1.38	<1	1.42
83	346.06	102.00	8.04	0.17	17.20	157.00	61.60	51.30	0.00	12.10	55.60	<20	<1	1.13	<1	2.97
84	230.85	68.70	4.40	0.54	10.80	119.00	27.30	113.00	0.00	4.71	45.60	<20	<1	<1	<1	12.50
85	360.39	92.30	9.91	0.08	25.40	178.00	54.50	199.00	0.00	26.00	101.00	22.90	<1	1.83	<1	3.60
86	374.83	105.00	8.94	0.04	22.40	177.00	61.40	53.90	0.00	23.30	79.50	<20	<1	1.56	<1	1.80
87	388.08	108.00	8.91	0.01	22.40	168.00	80.70	53.90	0.00	22.20	79.10	<20	<1	1.60	<1	1.25
88	386.06	106.00	9.03	0.04	22.80	171.00	77.00	189.00	0.00	16.10	83.60	<20	<1	1.29	<1	1.27
89	368.25	97.40	9.80	0.10	24.60	162.00	74.30	50.70	0.00	19.70	77.60	24.20	<1	1.40	<1	2.95
90	345.22	99.20	8.19	0.16	17.90	164.00	55.70	65.90	0.00	12.10	74.60	<20	<1	1.11	<1	2.24
91	358.95	104.00	8.70	0.12	19.70	183.00	43.30	129.00	0.00	19.80	82.20	<20	<1	1.42	<1	4.17
92	323.51	95.50	6.67	0.23	17.20	165.00	38.70	209.00	0.00	15.30	62.50	<20	<1	1.11	<1	5.21
93	343.61	113.00	9.93	0.34	10.80	190.00	19.50	41.80	0.00	9.66	41.40	<20	<1	1.67	<1	9.66
94	375.27	103.00	9.74	0.08	22.50	173.00	66.90	51.30	0.00	16.10	86.50	<20	<1	1.31	<1	1.51
95	347.54	92.00	7.78	0.12	22.30	157.00	68.20	135.00	0.00	16.00	76.80	22.60	<1	1.12	<1	3.59
96	344.06	93.20	8.28	0.15	20.70	159.00	62.60	127.00	0.00	13.70	70.00	21.30	<1	1.10	<1	4.23
97	362.51	98.70	9.27	0.08	23.00	181.00	50.20	253.00	0.00	25.30	89.80	<20	<1	1.72	<1	3.88
98	362.77	100.00	9.07	0.10	21.90	186.00	45.50	208.00	0.00	21.70	85.90	<20	<1	1.57	<1	3.96
99	359.24	95.50	9.46	0.09	23.50	181.00	49.50	193.00	0.00	22.50	84.70	<20	<1	1.58	<1	3.59
100	387.30	97.80	9.45	0.02	27.20	177.00	75.60	224.00	0.00	26.90	84.50	20.90	<1	1.75	<1	2.79
101	239.47	60.70	5.88	0.41	15.60	113.00	43.80	80.50	0.00	11.70	51.70	<20	<1	<1	<1	10.60
102	377.33	103.00	8.97	0.10	23.20	167.00	75.00	61.50	0.00	15.30	70.90	<20	<1	1.29	<1	2.17
103	264.53	83.50	6.27	0.65	11.30	147.00	15.70	110.00	0.00	7.44	41.70	<20	<1	<1	<1	18.20
104	366.25	95.30	10.90	0.14	24.00	187.00	48.70	206.00	0.00	27.60	83.60	20.50	<1	1.94	<1	3.58
105	354.36	102.00	7.74	0.14	18.30	166.00	60.10	79.80	0.00	16.50	63.00	<20	<1	1.11	<1	2.85
106	384.94	106.00	8.65	0.03	22.40	167.00	80.80	65.30	0.00	19.70	73.70	<20	<1	1.40	<1	1.36
107	376.44	111.00	8.20	0.08	17.80	170.00	69.30	54.50	0.00	12.70	61.50	<20	<1	1.88	<1	2.21
108	338.22	101.00	10.30	0.27	17.30	177.00	32.10	248.00	0.00	17.70	39.80	23.40	<1	1.47	<1	5.71

## References

- Zheng, M.P. Regional Distribution and Prospects of Potash in China. *Acta Geol. Sin.* **2010**, *84*, 1523–1553.
- Luo, T.; Zhang, Y.Q. Security assessment and early warning of potash resources in China. *Geol. J. China Univ.* **2022**, *37*, 575–587.
- Mao, X.; Li, J.H.; Liu, J.X. Tectonic Genetic Study of Global Potash Resource and Its Distribution. *Geol. J. China Univ.* **2017**, *23*, 9.
- Tan, H.T.; Sun, W.; Cui, Y.Z.; Wei, Q.Q.; Li, T.S.; Yan, D.Y. Present Situation of Potash Resources and Analysis of Development and Application of Polyhalite. *Inorg. Chem. Ind.* **2022**, *54*, 23–30.
- Ma, L.C.; Ma, J.Q.; Han, J.Q.; Liu, C.L.; Niu, L.; Zhang, Q. Characteristics and genesis of Southey potash deposit, Saskatchewan, Canada. *Miner. Depos.* **2014**, *33*, 12.
- Yang, G.W. Potash Deposites Geology of Saskatchewan Province in Canada. *China Well Rock Salt* **2013**, *44*, 23–25+31.
- Warren, J.K. Evaporites Through Time: Tectonic, Climatic and Eustatic Controls in Marine and Nonmarine Deposits. *Earth-Sci. Rev.* **2010**, *98*, 217–268. [[CrossRef](#)]
- Jensen, G.K.S.; Rostron, B.J.; Duke, M.J.M.; Holmden, C. Bromine and stable isotope profiles of formation water from potash mine-shafts, Saskatchewan, Canada. *J. Geochem. Explor.* **2006**, *89*, 170–173. [[CrossRef](#)]

9. Tang, M.; Liu, C.L.; Chen, Y.Z.; Cao, Y.T.; Hu, Y.N. Quantitative Analysis and Significance of the Marine Potash Deposits in the World. *Acta Sedimentol. Sin.* **2009**, *27*, 326–333.
10. Abdul, W.; Muhannad, I. *Potash Research in Pakistan—Potash Use and Dynamic in Agriculture*; Springer: Singapore, 2022; pp. 67–86.
11. Jones, C.L. *Potential for Potash and Other Evaporite Mineral Resources in West Pakistan*; USGS: Washington, DC, USA, 1968; pp. 68–153.
12. Tan, D.H.; Li, B.Y.; Zhang, M.M.; Wang, M.; Qi, C.J.; Zhang, X.; Wang, S.L.; Deng, Y.F.; Zhang, B.B.; Zhang, H.L. Study on Ore Controlling Structural Conditions of Walun Potash Deposits in Nakhon Basin, Thailand. *Geol. Chem. Miner.* **2021**, *43*, 307–314.
13. Qin, Z.J. *Geochemical Research on the Provenance and Sedimentary Characteristics of Potash Deposits in the Khorat Plateau*; Qinghai Institute of Salt Lakes, Chinese Academy of Sciences: Beijing, China, 2019.
14. Hite, R.J. *Potential for Potash and Related Mineral Resources Khorat Plateau, Northeast Thailand and Central Laos*; USGS: Washington, DC, USA, 1967; pp. 1–70.
15. Lowenstein, T.K. Origin of depositional cycles in a Permian “saline giant”: The Salado (McNutt zone) evaporites of New Mexico and Texas. *Geol. Soc. Am. Bull.* **1988**, *100*, 592–608. [[CrossRef](#)]
16. Kemp, S.J.; Smith, F.W.; Wagner, D.; Mounteney, I.; Bell, C.P.; Milne, C.J.; Gowing, C.J.B.; Pottas, T.L. An Improved Approach to Characterize Potash-Bearing Evaporite Deposits, Evidenced in North Yorkshire, United Kingdom. *Econ. Geol. Bull. Soc. Econ. Geol.* **2016**, *111*, 719–742. [[CrossRef](#)]
17. Kampschulte, A.; Buhl, D.; Strauss, H. The sulfur and strontium isotopic compositions of Permian evaporites from the Zechstein basin, northern Germany. *Geol. Rundsch.* **1998**, *87*, 192–199. [[CrossRef](#)]
18. Leitner, C.; Neubauer, F.; Genser, J.; Borojević-Šoštarić, S.; Rantitsch, G. *40Ar/39Ar Ages of Crystallization and Recrystallization of Rock-Forming Polyhalite in Alpine Rocksalt Deposits*; Interscience Publishers: Geneva, Switzerland, 2014.
19. Bojar, A.V.; Hałas, S.; Bojar, H.P.; Trembacowski, A. Multiple isotope tracers from Permian-Triassic hydrated sulfates: Implications for fluid-mineral interaction. *BSGF—Earth Sci. Bull.* **2019**, *190*, 11. [[CrossRef](#)]
20. Chen, A.D.; Gu, J.N.; Wang, X.F.; Han, G.; Li, H.P.; Yuan, W.H. Rethinking in correlation scheme between Late Quaternary evaporite-deposition period and glacial period in saline lakes of Qaidam Basin. *Miner. Depos.* **2022**, *41*, 426–439.
21. Li, J. *The Formation Mechanism of Polyhalite in Salt Lakes of Qaidam Basin—Taking Qarhan and Kuntanyi Salt Lakes as Examples*; Qinghai Institute of Salt Lakes, Chinese Academy of Sciences: Beijing, China, 2021.
22. Ma, Z.; Han, F.Q.; Yi, L.; Zhang, G.W.; Lu, S.C.; Lu, X.H.; Syed, A.H.; Sun, Y.Q.; Han, G.; Yuan, W.H. Sedimentary Characteristics and Assessment of Salt Mineral Resources in Kuntanyi Salt Lake, Qaidam Basin. *J. Salt Lake Res.* **2020**, *28*, 86–95.
23. Zheng, M.P. *Salt Lake on the Tibetan Plateau*; Science and Technology of China Press: Beijing, China, 1989.
24. Casas, E.; Lowenstein, T.K.; Spencer, R.J.; Zhang, P.X. Carnallite mineralization in the nonmarine, Qaidam Basin, China: Evidence for the early diagenetic origin of potash evaporites. *J. Sediment. Petrol.* **1992**, *62*, 881–898.
25. Wang, L.F.; Yu, Y.M.; Li, B.Y.; Zhang, F.K.; Deng, Y.F.; Li, W.X.; He, Q. Numerical simulation of brine in the Luobei depression mining area, Salt Lake, Lop Nur. *Miner. Explor.* **2022**, *13*, 797–806.
26. Wang, K.; Sun, M.G.; Ma, L.C.; Tang, Q.F.; Yan, H.; Zhang, Y. Spatial variability in the geochemical characteristics of the K-rich brines in the Lop Nur. *Acta Geol. Sin.* **2020**, *94*, 1183–1191.
27. Li, W.X.; Zhang, F.K.; Yu, Y.M.; Wang, J.; Ma, B.C.; Zhao, L.L.; Chen, W.; Yang, B.H. Preliminary Studies on Variation Regulation and Genetic of Hydrologic Parameter of Brine Reservoirs in Playa Lop Nur during Potash Exploitation. *J. Salt Lake Res.* **2018**, *26*, 44–51.
28. Ma, L.C.; Li, B.G.; Jiang, P.A. Dissolution and Migration of main geochemical elements in the salt crust of Lop Nur Dry Salt Lake. *Miner. Depos.* **2010**, *29*, 385–386.
29. Ma, L.C.; Li, B.G.; Zhong, J.P.; Sheng, J.D.; Wu, H.Q. Geochemical characteristics and enrichment mechanism of potassium in Lop Nur ‘Great Ear’ playa. *Miner. Depos.* **2010**, *29*, 616–624.
30. Liu, C.L.; Wang, M.L.; Jiao, P.C.; Chen, Y.Z. The Probing of Regularity and Controlling Factors of Potash Deposits Distribution in Lop Nur Salt Lake, Xinjiang. *Acta Geosci. Sin.* **2009**, *30*, 796–802.
31. Wang, M.L. *Potassium Salt Resources in Lop Nur Salt Lake*; Geology Press: Beijing China, 2001.
32. Yu, X.C.; Wang, C.L.; Huang, H.; Wang, J.Y. Origin and Evolution of Deep-Seated K-Rich Brine in Paleogene of Qianjiang Depression, Hubei Province. *Earth Sci.* **2022**, *47*, 122–135.
33. Ma, L.C.; Huang, H.; Zhang, L.Y.; Liu, C.L.; Sun, M.G.; Niu, L. Characteristics of Paleogene. *Acta Geol. Sin.* **2015**, *89*, 2114–2121.
34. Liu, C.L.; Wang, C.L.; Xu, H.M.; Liu, B.K.; Shen, L.J.; Wang, L.C.; Zhao, Y.J. Research progress of potassium-bearing minerals in Paleogene evaporites in Jiangling Depression. *Miner. Depos.* **2013**, *32*, 221–222.
35. Zhang, B.; Liu, W.; Yang, K.; Pei, W.B.; Zhang, S.M.; Xiao, W. Salt Accumulation, Potassium Formation Mechanism and Enrichment Model of Triassic in Northeast Sichuan Basin. *Earth Sci.* **2022**, *47*, 15–26.
36. Chen, X.E.; Zhang, B.; Fan, K.; Yang, K.; Zhang, S.M. Metallogenic model for the coexistence of potassium-rich brine and natural gas in the same strata: An example from the Middle Triassic Leikoupo Formation in the Moxi Anticline, Central Sichuan Basin, Southwest China. *Earth Sci. Front.* **2021**, *28*, 79–94.
37. Bian, S.J.; Liu, X.; Dong, Y.P.; Li, W. Potassium extraction from potassium-rich brine in Puguang region, northeastern Sichuan, China. *Earth Sci. Front.* **2021**, *28*, 171–178.
38. Shang, W.J.; Zhang, Y.S.; Li, K.; Xing, E.Y.; Gui, B.L.; Peng, Y.; Zhao, H.T. Geochemical characteristics of a new type of polyhalite potassium ore deposits in Xuanhan area, northeast Sichuan, and their significance. *Miner. Depos.* **2020**, *39*, 369–380.

39. Song, G.; Miao, Z.Y.; Du, S.R.; Li, X.M. Geochemical Characteristics of Trace Elements before and after the upper Salt Forming Period of the MK-3 Core, Simao Basin and Their Paleoenvironment Implications. *Acta Geosci. Sin.* **2022**, *43*, 584–592.
40. Yan, M.D.; Zhang, D.W.; Li, M.H. Research progress and new views on the potash deposits in the Simao and Khorat Basin. *Earth Sci. Front.* **2021**, *28*, 10–28.
41. Miao, Z.Y.; Zheng, M.P.; Lou, P.C.; Zhang, X.F.; Sun, H.T.; Zhang, Z.; Xu, Q.H.; Du, X.M. The deep source and shallow mineralization model of potash deposits in the Simao Basin: Evidence from Sr isotope. *Geol. China* **2022**, *49*, 1923–1935.
42. Miao, Z.Y.; Zheng, M.P.; Zhang, X.F.; Zhang, Z.; Gao, Y.Z. Geochemistry of sulfur isotope in evaporite and its sedimentology significance: A case study from the well MZK-3 in the Simao basin, southwestern China. *Acta Geol. Sin.* **2019**, *93*, 1166–1179.
43. Sun, P.X. The Exportation and Utilization of Yncheng Salt Lake Resources. *J. Salt Lake Res.* **2007**, *15*, 5.
44. Gong, D.X. *Sedimentary Characteristics of the Oligocene Salt-Bearing Formation and Prospect of Potash Resources in Hoh Xil Basin*; Chengdu University of Technology: Chengdu, China, 2011.
45. Xu, J.X.; Ma, H.Z.; Yang, L.S.; Tan, H.B.; Wang, J.G. Paleogene and Neogene Tectonic Environment and Sedimentation of Evaporite in Kuqa Basin. *Acta Geol. Sin.* **2006**, *80*, 9.
46. Xu, Y. *Provenance, Ancient Water Temperature, Degree of Evaporation of Paleogene Salt Lake and Evaluation of Potassium-Forming Perspective in the Kuqa Basin, Xin Jiang*; China Academy of Geological Sciences: Beijing, China, 2018.
47. Sun, M.G.; Ma, L.C. Potassium-rich brine deposit in Lop Nor basin, Xinjiang, China. *Sci. Rep.* **2018**, *8*, 7676. [[CrossRef](#)] [[PubMed](#)]
48. Ma, L.; Lowenstein, T.K.; Li, B.; Jiang, P.; Liu, C.; Zhong, J.; Sheng, J.; Qiu, H.; Wu, H. Hydrochemical characteristics and brine evolution paths of Lop Nor Basin, Xinjiang Province, Western China. *Appl. Geochem.* **2010**, *25*, 1770–1782. [[CrossRef](#)]
49. Shi, W.; Liu, C.L.; Yang, H.J.; Ma, Y.S.; Xie, A.G.; Gu, Y.Q.; Gong, M.Q.; Du, J.J.; Shi, J. Research on Neotectonics of the Lop Nur Basin Based on Sandbox Experiments. *Geotecton. Metallog.* **2009**, *33*, 6.
50. Shi, W.; Tian, M.; Ma, Y.S.; Gong, M.Q.; Du, J.J.; Liu, Y. A Numerical Simulating Research on Neotectonics in the Lop Nur Basin. *J. Geomech.* **2011**, *17*, 9.
51. Guo, Z.J.; Zhang, Z.C. The Geological interpretation of the forming and evolution of Lop Nur, NW China. *Geol. J. China Univ.* **1995**, *1*, 6.
52. Luo, C. *The Environmental Change in Lop Nur, Xinjiang During Late Last Glacial and Response to Global Change*; University of Science and Technology of China: Hefei, China, 2008.
53. Luo, C.; Peng, Z.C.; Yang, D.; Liu, W.G.; He, J.F.; Liu, G.J. Research on the Environmental Evolution of Lop Nur in Xinjiang, China. *Chin. J. Nat.* **2006**, *28*, 37–41. [[CrossRef](#)] [[PubMed](#)]
54. Zheng, M.P.; Qi, W. Preliminary Analysis of the Sedimentary Environment and Potassium Prospecting Prospect in Lop Nur Salt Lake Since Late Pleistocene. *Chin. Sci. Bull.* **1991**, *36*, 4.
55. Wang, H.Z.; Yang, S.N.; Liu, B.P. *Tectonic Palaeogeography and Biopalaeogeography of China and Its Adjacent Areas*; China University of Geosciences Press: Wuhan, China, 1990.
56. Tang, L.J.; Qiu, H.J.; Yun, L.; Yang, Y.; Huang, T.Z.; Wang, P.H.; Xie, D.Q.; Li, M.; Jiang, H.S. Analysis of basin-mountain coupling and transition of the Northern Tarim Basin–Southern Tianshan Orogenic Belt. *Earth Sci. Front.* **2012**, *19*, 10.
57. Xu, Z.Q.; Li, S.T.; Zhang, J.X.; Yang, J.S.; He, B.Z.; Li, H.B.; Lin, C.S.; Cai, Z.H. Paleo-Asian and Tethyan Tectonic Systems with Docking the Tarim Block. *Acta Petrol. Sin.* **2011**, *22*, 1–21.
58. Wang, B.Q.; Huang, Z.B.; Ma, P.I.; Pan, Z.Z.; Wang, L.L. Establishment of Division Standard, Evidence and Principle of Structural Units in Tarim Basin. *Geotecton. Metallog.* **2009**, *33*, 86–93.
59. Wu, B. *Transformation of Critical Tectonic Regimes and Its Mechanisms in Eastern Tarim Basin: Implications for Tectonic Controls on Oil and Gas Occurrence*; China University of Geosciences: Beijing, China, 2015.
60. Liu, D.L.; Li, Z.S.; Wu, X.Q.; Tao, S.Z. The Traces of Nearly North-south Structures in the Tarim Basin. *Acta Geol. Sin.* **2007**, *81*, 8.
61. Han, F.F.; Shi, D.Y.; Sun, Z.W. Brief Introduction on Structure and Water Control in Northern Lop Nur, Xinjiang. *West-China Explor. Eng.* **2013**, *25*, 174–176.
62. Ma, L.C.; Wang, K.; Zhang, Y.; Tang, Q.F.; Sun, M.G. Abnormal Enrichment Mechanism of Potassium-rich Brine Deposit in Lop Nor Basin of Xinjiang. *Earth Sci.* **2022**, *47*, 72–81.
63. Li, B.Y.; Zhang, F.K.; Deng, Y.F.; Yu, Y.M.; Dong, L.B.; Li, W.X.; Wang, L.F.; Ma, B.C. Geological Characteristics and Genesis of the Solid Potash Salt Deposit in the NO.3 Fault Depression Zone in Northwest Lop Nur. *J. Salt Lake Res.* **2022**, *30*, 63–71.
64. Li, W.X. Distribution Characteristics and Mining Laws Discussion of the Low-Grade Carnallite in Lop Nur. *Geol. Chem. Miner.* **2016**, *38*, 93–98.
65. Wang, K. *Geochemical Characteristics and Provenance Analysis of Brine in Lop Nor Playa, Xinjiang*; China University of Geosciences: Beijing, China, 2020.
66. Ma, L.; Wang, K.; Zhang, Y.; Tang, Q.; Yan, H. Dynamic variations in salinity and potassium grade of a potassium-rich brine deposit in lop nor basin, China. *Sci. Rep.* **2021**, *11*, 3351–3364. [[CrossRef](#)]
67. Lowenstein, T.K.; Spencer, R.J.; Pengxi, Z. Origin of ancient potash evaporites: Clues from the modern nonmarine qaidam basin of western China. *Science* **1989**, *245*, 1090–1092. [[CrossRef](#)] [[PubMed](#)]
68. Lowenstein, T.K.; Risacher, F. Closed Basin Brine Evolution and the Influence of Ca–Cl Inflow Waters: Death Valley and Bristol Dry Lake California, Qaidam Basin, China, and Salar de Atacama, Chile. *Aquat. Geochem.* **2009**, *15*, 71–94. [[CrossRef](#)]
69. Lei, Y.C.; Xu, Z.Q. the Effects of Ground CaCl<sub>2</sub> Type Brine on Potassium Salts Deposits of Charhen Salt Lake. *J. Salt Lake Res.* **1999**, *7*, 8.

70. Stewart, F.H. The Mineralogy of the British Permian Evaporites. *Mineral. Mag.* **1965**, *34*, 460–470. [[CrossRef](#)]
71. Harville, D.G.; Fritz, S.J. Modes of diagenesis responsible for observed succession of potash evaporites in the Salado Formation, Delaware Basin, New Mexico. *J. Sediment. Petrol.* **1986**, *56*, 648–656.
72. Harvie, C.E.; Weare, J.H. The prediction of mineral solubilities in natural waters: The Na-K-Mg-Ca-Cl-SO<sub>4</sub>-H<sub>2</sub>O system from zero to high concentration at 25 °C. *Geochim. Cosmochim. Acta* **1980**, *44*, 981–997. [[CrossRef](#)]
73. Rahimpour-Bonab, H.; Shariatinia, Z.; Siemann, M.G. Origin and geochemistry of Miocene marine evaporites associated with red beds: Great Kavir Basin, Central Iran. *Geol. J.* **2007**, *42*, 37–54. [[CrossRef](#)]
74. Pena, J.A.; Garcia-Ruiz, J.M.; Marfil, R.; Prieto, M. Growth features of magnesium and sodium salts in a recent Playa Lac of La Mancha (Spain). *Estud. Geol.* **1982**, *38*, 245–257.
75. Sinha, R.; Raymahashay, B.C. Evaporite mineralogy and geochemical evolution of the Sambhar Salt Lake, Rajasthan, India. *Sediment. Geol.* **2004**, *166*, 59–71. [[CrossRef](#)]
76. Warren, J.K. *Evaporite Sedimentology: Importance in Hydrocarbon Accumulation*; Prentice Hall: Englewood Cliffs, NJ, USA, 1989; pp. 1–37.
77. Peryt, T.M.; Pierre, C.; Gryniv, S.P. Origin of polyhalite deposits in the Zechstein (Upper Permian) Zdrada platform (northern Poland). *Sedimentology* **1998**, *45*, 565–578. [[CrossRef](#)]
78. Ayora, C.; Garcia-Veigas, J.; Pueyo, J.J. The chemical and hydrological evolution of an ancient potash-forming evaporite basin as constrained by mineral sequence, fluid inclusion composition, and numerical simulation. *Geochim. Cosmochim. Acta* **1994**, *58*, 3379–3394. [[CrossRef](#)]
79. Hardie, L.A. The origin of the Recent non-marine evaporite deposit of Saline Valley, Inyo County, California. *Geochim. Cosmochim. Acta* **1968**, *32*, 1279–1301. [[CrossRef](#)]
80. Braitsch, O. *Salt Deposits: Their Origin and Composition*; Burek, P.J.; Nairn, A.E.M.; Herrmann, A.G.; Evans, R., Translators; Springer: Berlin/Heidelberg, Germany, 1971.
81. Estefan, S.F.; Awadalla, F.T.; Yousef, A.A. Solar evaporation of Qarun Lake brine. *Salt Res. Ind.* **1980**, *16*.
82. Ordóñez, S.; Sánchez-Moral, S.; García del Cura, M.A.; Badiola, E.R. Precipitation of salts from a Mg, Na, SO<sub>4</sub>, Cl playa lake brines: Endorreic saline ponds of La Mancha, Central Spain. *Soc. Econ. Mineral. Paleontol. Spec. Publ.* **1994**, *67*, 913–922.
83. Christoph, L.; Sebastian, W.; Mathias, H.; Albert, G.; Friedrich, F.; Franz, N. Alpine halite-mudstone-polyhalite tectonite: Sedimentology and early diagenesis of evaporites in an ancient rift setting (Haselgebirge Formation, eastern Alps). *GSA Bull.* **2017**, *129*, 1537–1553.
84. Huang, X.Z. Hydrogeologic Conditions for Preservation of the Nongle Polyhalite ore. *Hydrogeol. Eng. Geol.* **2004**, *31*, 111–114.
85. Li, M.; Fang, X.; Galy, A.; Wang, H.; Song, X.; Wang, X. Hydrated sulfate minerals (bloedite and polyhalite): Formation and paleoenvironmental implications. *Carbonates Evaporites* **2020**, *35*, 126. [[CrossRef](#)]
86. Niu, X.; Jiao, P.C.; Cao, Y.T.; Zhao, Y.J.; Liu, B.S. the Origin of Polyhalite and Its Indicating Significance for the Potash Formation in the Bieletan Area of the Qarhan Salt Lake, Qinghai. *Acta Geol. Sin.* **2015**, *89*, 9.

**Disclaimer/Publisher's Note:** The statements, opinions and data contained in all publications are solely those of the individual author(s) and contributor(s) and not of MDPI and/or the editor(s). MDPI and/or the editor(s) disclaim responsibility for any injury to people or property resulting from any ideas, methods, instructions or products referred to in the content.